Picalm, a novel regulator of GLUT4-trafficking in adipose tissue

Jasmin Gaugel[1,2], Neele Haacke[1,2], Ratika Sehgal[1,2], Markus Jähnert[1,2], Wenke Jonas [1,2], Anne Hoffmann[3], Matthias Blüher[2,3,4], Adhideb Ghosh[5], Falko Noé[5], Christian Wolfrum[5], Joycelyn Tan[6], Annette Schürmann[1,2,7], Daniel J. Fazakerley[6], Heike Vogel[1,2,*]

ABSTRACT

Objective: *Picalm* (phosphatidylinositol-binding clathrin assembly protein), a ubiquitously expressed clathrin-adapter protein, is a well-known susceptibility gene for Alzheimer's disease, but its role in white adipose tissue (WAT) function has not yet been studied. Transcriptome analysis revealed differential expression of *Picalm* in WAT of diabetes-prone and diabetes-resistant mice, hence we aimed to investigate the potential link between *Picalm* expression and glucose homeostasis, obesity-related metabolic phenotypes, and its specific role in insulin-regulated GLUT4 trafficking in adipocytes.

Methods: *Picalm* expression and epigenetic regulation by microRNAs (miRNAs) and DNA methylation were analyzed in WAT of diabetes-resistant (DR) and diabetes-prone (DP) female New Zealand Obese (NZO) mice and in male NZO after time-restricted feeding (TRF) and alternate-day fasting (ADF). *PICALM* expression in human WAT was evaluated in a cross-sectional cohort and assessed before and after weight loss induced by bariatric surgery. siRNA-mediated knockdown of *Picalm* in 3T3-L1-cells was performed to elucidate functional outcomes on GLUT4-translocation as well as insulin signaling and adipogenesis.

Results: *Picalm* expression in WAT was significantly lower in DR compared to DP female mice, as well as in insulin-sensitive vs. resistant NZO males, and was also reduced in NZO males following TRF and ADF. Four miRNAs (let-7c, miR-30c, miR-335, miR-344) were identified as potential mediators of diabetes susceptibility-related differences in *Picalm* expression, while 11 miRNAs (including miR-23a, miR-29b, and miR-101a) were implicated in TRF and ADF effects. Human *PICALM* expression in adipose tissue was lower in individuals without obesity vs. with obesity and associated with weight-loss outcomes post-bariatric surgery. siRNA-mediated knockdown of *Picalm* in mature 3T3-L1-adipocytes resulted in amplified insulin-stimulated translocation of the endogenous glucose transporter GLUT4 to the plasma membrane and increased phosphorylation of Akt and Tbc1d4. Moreover, depleting Picalm before and during 3T3-L1 differentiation significantly suppressed adipogenesis, suggesting that Picalm may have distinct roles in the biology of pre- and mature adipocytes.

Conclusions: Picalm is a novel regulator of GLUT4-translocation in WAT, with its expression modulated by both genetic predisposition to diabetes and dietary interventions. These findings suggest a potential role for Picalm in improving glucose homeostasis and highlight its relevance as a therapeutic target for metabolic disorders.

1. INTRODUCTION

White adipose tissue (WAT), once considered merely a fat storage depot, is also recognized as an endocrine organ, playing a central role in whole-body metabolism, and obesity-driven WAT dysfunction is one of the main causes of type 2 diabetes (T2D). Although only about 5% of postprandial glucose is taken up by the adipose tissue [1], the uptake of glucose into fat cells plays a crucial role in lipid handling [2]. Defects in insulin-stimulated glucose uptake into adipocytes can disturb lipid metabolism, often accompanied by an impaired insulin-induced

[1]Research Group Nutrigenomics of Obesity and Department of Experimental Diabetology, German Institute of Human Nutrition Potsdam-Rehbruecke, Nuthetal, Germany [2]German Center for Diabetes Research (DZD e.V.), München, Neuherberg, Germany [3]Helmholtz Institute for Metabolic Obesity and Vascular Research (HI-MAG), Helmholtz Zentrum München, University of Leipzig and University Hospital Leipzig, Leipzig, Germany [4]Medical Department III-Endocrinology, Nephrology, Rheumatology, University of Leipzig Medical Center, Leipzig, Germany [5]Laboratory of Translational Nutrition Biology, Institute of Food, Nutrition and Health, ETH Zürich, Schwerzenbach, Switzerland [6]Metabolic Research Laboratories, Institute of Metabolic Science, University of Cambridge, Cambridge, CB2 0QQ, United Kingdom [7]Institute of Nutritional Sciences, University of Potsdam, Nuthetal, Germany

*Corresponding author. German Institute of Human Nutrition Potsdam-Rehbruecke, Research Group Nutrigenomics of Obesity and Department of Experimental Diabetology, Arthur-Scheunert-Allee 114-116, 14558, Nuthetal, Germany. E-mail: heikevogel@dife.de (H. Vogel).

suppression of lipolysis [2]. As a result, elevated circulating free fatty acids can lead to ectopic fat storage in other organs, and thereby promote insulin resistance e.g. in skeletal muscle and liver [2]. In recent years, it has been appreciated that insulin resistance and associated metabolic derangements are presumably mainly attributed to disrupted insulin-stimulated glucose uptake via GLUT4, rather than to defects in proximal insulin signaling [2,3]. Consequently, elucidating the GLUT4 trafficking machinery represents a promising avenue for discovering new therapeutic targets.

Mouse strains with a genetic predisposition to a diabetes-like phenotype are a valuable tool to screen for potential candidates involved in T2D pathology. Previous work by our group has shown in male NZO mice, a model of polygenetic obesity and T2D [4], that implementing time-restricted feeding and alternate-day fasting are effective in diminishing ectopic fat storage in liver, skeletal muscle, and pancreas and prevent the development of T2D [5,6]. Interestingly, female NZO mice show varying susceptibility to diabetes development when fed a diabetogenic diet containing 60 kcal% from fat [7,8]. These models thus provide the opportunity to search for genes involved a) in diabetes prevention by dietary restriction and b) in diabetes predisposition.

Transcriptome analysis identified *Picalm* (phosphatidylinositol-binding clathrin assembly protein) as one of the genes with the strongest expression difference in adipose tissue of female diabetes-prone (DP) and diabetes-resistant (DR) NZO mice. *Picalm* encodes a clathrin assembly protein involved in clathrin-mediated endocytosis and the internalization of SNARE-proteins. So far, research has mainly focused on the role of Picalm in Alzheimer's disease, as genome-wide association studies (GWAS) have identified it as one of the most significant susceptibility loci for this pathology. Following this discovery, effects of *Picalm* in the neuronal context have been intensively studied, primarily in relation to amyloid β plaques and tau pathology [9].

In this study, our objective was to explore whether there is a mechanistic link between reduced expression of Picalm in adipose tissue and improvement in glucose homeostasis, and also to clarify the extent to which the altered expression of this gene is regulated by epigenetic mechanisms. By integrating these approaches, we aimed to provide a deeper understanding of the role of Picalm in metabolic regulation and its potential as a therapeutic target for obesity and T2D.

2. MATERIALS AND METHODS

2.1. Animal studies

2.1.1. Diabetes-prone and diabetes-resistant NZO mice
Female New Zealand Obese (NZO/HlBomDife) mice from in-house breeding (German Institute of Human Nutrition Potsdam-Rehbruecke, Germany) were fed a high-fat diet (60 kcal% from fat; D12492, Research Diets, USA) starting at the age of 5 weeks until 10 weeks as previously described [10,11]. Animals were classified into DP and DR status based on final blood glucose levels between ≥ 8.8 mM and <16.6 mM, and liver fat content <55.2 HU (Hounsfield units), both at the age of 10 weeks, which was described in detail in previous studies [11,12]. Male NZO (NZO/HlBomDife) mice were fed *ad libitum* with a high-fat diet (HFD, 49 kcal% from carbohydrate, 33 kcal% from fat and 18 kcal% from protein, S8022-E080 unsat. FA, Ssniff, Soest, Germany) starting at 15 weeks of age and were sacrificed 9 weeks later. Body weight and blood glucose levels were measured weekly.

A second subgroup of male NZO/HlBomDife mice were used and housed as described previously [13]. Briefly, starting at the age of 3 weeks onward, all mice received a carbohydrate-free diet (HFD-CH, Altromin C105789). At the age of 18 ± 1 weeks, one subgroup of animals was sacrificed for tissue collection and later expression analysis. Another subgroup received a carbohydrate-containing diet (HFD+CH, self-made with 40 kcal% from carbohydrates) for 16 days and were then sacrificed. Control male NZO/HlBomDife mice were kept on standard diet until week 8 (V153x R/M-H; ssniff, Soest, Germany). B6-*ob/ob* and C57BL/6J mice — B6.V-*Lep^{ob/ob}*/JBomTac (B6-*ob/ob*) and C57BL/6J male mice (Charles River Laboratories, Italy) were placed on a high-fat diet (D12492, Research Diets, USA) before sacrificing at the age of 22 weeks.

2.1.2. Time-restricted feeding and alternate-day fasting in NZO mice
Male NZO/HlBomDife mice, from in-house breeding, were fed a high-fat diet (S8022-E080 unsat. FA; Ssniff, Germany) for one week starting at three weeks of age. After this period, mice were randomly assigned to one of three groups: *ad libitum* (AL), TRF, or ADF, as previously described [5].

All animals were kept in a 12:12 h light—dark cycle at 22 ± 1 °C and all animal experiments were approved by the ethics committee of the State Agency of Environment, Health and Consumer Protection (State of Brandenburg, Germany; ethics approvals: V3-2347-31-2011, V3-2347-23-2012, 2347-28-2014, 2347-50-2019, 2347-01-2022-26-G). All methods used in animal experiments were carried out in accordance with relevant guidelines, and handled according to standard use protocols and animal welfare regulations, and we also confirmed that all animal methods were reported in accordance with ARRIVE guidelines (http://arriveguidelines.org).

2.2. Human cohorts
Human data were obtained from the Leipzig Obesity BioBank (LOBB; https://www.helmholtz-munich.de/en/hi-mag/cohort/leipzig-obesity-bio-bank-lobb). We enrolled a consecutively recruited cross-sectional cohort consisting of 1449 patients with obesity (70% women; mean $\pm$ standard deviation: age $= 46.9 \pm 11.7$ years, BMI $= 49.2 \pm 8.3$ kg/m^2) and 31 patients without obesity (52% women; age $= 55.6 \pm 13.4$ years, BMI $= 25.7 \pm 2.7$ kg/m^2). Plasma parameters including C-reactive protein (CRP)- and Interleukin-6 (IL6)-levels were measured as described previously [14].

Furthermore, we included a longitudinal bariatric surgery cohort (BSC) to investigate expression differences related to body weight loss, including 65 individuals with morbid obesity (70% women; BMI > 38 kg/m^2) who underwent a two-step bariatric surgery approach. The study was approved by the Ethics Committee of the University of Leipzig (approval no: 159-12-21052012) and was performed in accordance with the Declaration of Helsinki. All participants gave written informed consent before taking part in the study and have been informed of the purpose, risks and benefits of the biobank. A detailed description of this cohort can be found in Supplementary data.

2.3. RNA extraction and transcriptome analysis in adipose tissue
Total RNA was extracted from gonadal white adipose tissue (WAT) of the different mouse models using the miRNeasy kit (Qiagen, Germany) as per the manufacturer's instructions with DNase treatment and quantified using 2100 Bioanalyzer (Agilent Technologies, Germany) (DP, DR n = 15; AL, TRF, ADF n = 5). The RNA samples were sequenced by BGI (Shenzen, China) using BGISEQ. Raw sequencing reads after adapter trimming were aligned to reference genome GRCm38.p6_Ensemble100 via STAR v2.7.4a (DP, DR) or STAR v2.7.9a (AL, TRF, ADF) [15]. For normalization, FPKM values (Fragments Per Kilobase per Million mapped fragments) were calculated from raw

reads. For DP vs. DR, differential expression analysis was done using DESeq2 v1.34.0 [16] in R v.4.1.2 (www.R-project.org) with adjustment for multiple testing using Benjamini-Hochberg. The calculation of differential expression for TRF compared to AL, and ADF compared to AL was conducted using student's t-test with Welch's correction.

To generate human data from the LOBB, RNA was extracted from visceral adipose tissue (VIS) samples using the SMARTseq protocol [17,18]. For details, see Supplementary data.

For the correlation of adipogenesis- and inflammation-related genes to *Picalm* expression within the different RNA-seq datasets, the genes annotated to the Gene Ontology (GO) terms associated with cellular response to insulin stimulus (GO:0032869), fat cell differentiation (GO:0045444) and inflammatory response (GO:0006954) were downloaded from the Gene Ontology Browser (https://www.informatics.jax.org/vocab/gene_ontology). Differentially expressed genes ($p < 0.05$) in the DP vs. DR and TRF or ADF vs. AL groups overlapping with these GO terms were subsequently analyzed for correlation (R package stats v4.2.1, lm function) with *Picalm* expression.

2.4. Western blot analysis

Protein lysates were prepared from murine and human adipose tissue samples using RIPA buffer containing protease and phosphatase inhibitors (Thermo Fisher Scientific) and 13—15 μg protein were used for western blot using specific antibodies (primary antibody Picalm: HPA019053, Sigma; secondary antibody: P/N 926-32213, LiCOR). For normalization, total protein stain was conducted using Revert™ 700 Total Protein Stain (LiCOR).

2.5. miRNA analysis and target prediction in adipose tissue

2.5.1. Diabetes-prone and diabetes-resistant female NZO mice

Small RNA sequencing (RNA-seq) was performed (DR n = 14, DP n = 15) using BGISEQ-500 (DNBSEQ-G50 Sequencing V.1) technology from BGI (Shenzen, China). Low-quality reads, adapters, and other contaminants (5′ primer contaminants, no-insert tags, oversized insertion tags, low-quality tags, poly A tags and small tags, tags without 3′ primer) were excluded from the raw data, filtering only clean tags as FASTQ files. Bowtie2 was used to map these reads to the reference mouse genome (*Mus musculus mm10*) and other small RNA databases (MiRbase, pirnabank, Rfam). Prediction of microRNAs (miRNAs) was performed using miRDeep2. All steps were performed by BGI. The annotated miRNAs were then subjected to differential expression analysis using EdgeR v3.36.0 with adjustment for multiple testing (Benjamini-Hochberg).

2.5.2. Time-restricted feeding and alternate-day fasting in NZO mice

Total RNA (AL, TRF, ADF n = 5) was used to construct a small RNA (sRNA) library, which was sequenced on Illumina sequencing platform with SE50 performed by Novogene GmbH (Munich, Germany). For miRNA expression analyses, first the quality control and reads mapping to the reference sequence (*M. musculus mm10*) was performed. Known miRNAs were aligned using miRBase as reference [19]. Additionally, tags originating from protein-coding genes, repeat sequences, rRNA, tRNA, snRNA, and snoRNA were removed. The miRNA read counts were normalized as Transcripts Per Million (TPM) due to the library size (sample miRNA read count). DESeq2 v1.24.0 and EdgeR v3.24.3 were used to calculate the differential expression level. For all murine miRNA analyses, the databases mirTarBase 8.0 [20], DIANA-TarBase v8 [21], and miRecords [22] were used for target

prediction, whereby only experimentally validated miRNA targets were considered.

2.6. Genome-wide DNA methylation profiling

Genomic DNA was isolated from WAT (75 mg; AL, ADF n = 4; TRF n = 5; DP, DR n = 6) using the ReliaPrep™ gDNA Tissue Miniprep System (Promega, USA). According to the manufacturer's protocol, DNA methylation was measured using the Illumina Infinium Mouse Methylation BeadChip MM285 (Illumina, USA) performed by Life&Brain GmbH (Bonn, Germany). In brief, 2 μg genomic DNA was bisulfite converted. The bisulfite converted samples were amplified, fragmented and hybridized onto the array chip and scanned according to the standard protocol. The generated raw IDAT files were preprocessed using SeSAMe v1.14.2 R package. This encompassed the steps of preprocessing and quality control following the established preprocessing workflow including the functions qualityMask (Q), inferInfiniumIChannel (C), dyeBiasNL (D), pOOBAH (P), and noob (B) [23,24]. The Infinium Methylation BeadChip manifest and annotation data were obtained from zwdzwd.github.io/InfiniumAnnotation/ and merged to the data file. Finally, the limma v3.50.1 R package [25] was utilized to identify differentially methylated probes by applying a mixed linear model to the β values. DNA methylation probes were considered as significant at a $p < 0.05$.

2.7. Real-time quantitative PCR (RT-qPCR)

For real-time quantitative PCR, RNA extracted from WAT was reverse transcribed (M-MLV RT, Promega) and *Picalm* gene expression was measured and normalized to the housekeeping gene *Tbp* using specific probes (*Picalm*: Mm.PT.58.43171691, *Tbp*: Mm.PT.39a.22214839; Integrated DNA Technologies IDT, USA).

To validate the efficiency of siRNA-mediated knockdown in 3T3-L1 cells, RNA was extracted using the RNeasy Mini kit (Qiagen), cDNA was synthesized using M-MLV Reverse Transcriptase and for experiments on mature 3T3-L1 adipocytes, RT-qPCR was performed using the TaqMan Gene Expression Assay (*Picalm*: Mm00525455_m1) or the SYBR Green method (Thermo Fisher Scientific, USA). Gene expression was normalized to housekeeping genes (*Actin, 36B4*, and *18s rRNA*). qPCR assays used for expression analysis of *Picalm* and adipogenesis marker throughout 3T3-L1 differentiation were purchased from IDT (*Picalm*: Mm.PT.58.43171691; *Pparg*: Mm.PT.58.31539421; *Cebpa*: Mm.PT.58.30061639.g; *Fabp4*: Mm.PT.58.43866459; *Slc2a4*: Mm.PT.58.9683859) and normalized to the housekeeping gene *Tbp* (Mm.PT.39a.22214839).

For the analysis of miRNA expression in 3T3-L1 cells, reverse transcription of total RNA was performed using the miRCURY LNA RT Kit (Qiagen). For real-time PCR, the miRCURY LNA SYBR® Green PCR Kit (Qiagen) was used and miRNA expression of miR-30c-5p, miR-344-3p, miR-335-5p, miR-186-5p and miR-30b-5p (YP00204783, YP00205008, YP02119293, YP00206053, YP00204765, Qiagen) were measured and normalized to 5S rRNA (YP00203906, Qiagen).

2.8. GLUT4-translocation and insulin signaling assay in 3T3-L1 cells

3T3-L1 fibroblasts were provided by David E. James (University of Sydney, Australia), originally from Howard Green (Harvard Medical School, Boston, MA). Fibroblasts were cultured in high glucose DMEM supplemented with 10% fetal bovine serum (FBS) and 2 mM Glutamax (DMEM/FBS/Glutamax) at 37 °C in 10% CO_2. For differentiation into adipocytes, confluent fibroblasts were cultured in DMEM/FBS/Glutamax containing an adipogenic cocktail (350 nM insulin, 0.5 mM 3-

isobutyl-1-methylxanthine, and 250 nM dexamethasone for three days), followed by three days in DMEM/FBS/Glutamax and 350 nM insulin. Differentiated adipocytes were maintained in DMEM/FBS/ Glutamax. siRNA treatment was performed six days after initiation of differentiation (for detailed description see Supplementary data).

Adipocytes were used for experiments 9—10 days after the onset of differentiation. GLUT4-translocation assay was performed as described in [26]. In summary, adipocytes were serum-starved in DMEM containing 0.2% BSA for 2 h at 37 °C before stimulation with 0.5 nM or 100 nM insulin for 20 min. Cells were instantly fixed with 4% para-formaldehyde, quenched with 50 mM glycine, blocked (5% normal swine serum (NSS) in PBS) and incubated with anti-GLUT4 (LM048) (2 μg/mL, Integral Molecular, USA) and anti-TfR antibody (CD71) diluted 1:500 (14-0711-82; Thermo Fisher Scientific). Secondary antibodies (Alexa488-conjugated anti-human and Alexa647-conjugated anti-Rat; 1:500, Thermo Fisher Scientific), and Hoechst 33342 (1:5000) were applied at RT for 1 h. Imaging was performed with the Opera Phenix (Perkin Elmer) using a 20× NA1.0 water immersion objective. Nine fields of view were imaged per well and analyzed using a custom pipeline in Harmony High-Content Imaging and Analysis Software (Perkin Elmer; USA).

To assess insulin signaling, adipocytes in 24-well plates were cultured in 250 μL media for 48 h before being serum-starved in DMEM containing 0.2% BSA for 2 h at 37 °C, 10% CO_2, and then stimulated with 0.5 or 100 nM insulin for 20 min. Cells were washed three times with ice-cold PBS and lysed in RIPA buffer containing protease and phosphatase Inhibitors (Thermo Fisher Scientific). Lysates were soni-cated, centrifuged at $16,000 \times g$ at 4 °C for 20 min, protein concentration was quantified using the BCA Assay (Thermo Fisher Scientific) and 10—20 μg of protein was used for SDS-PAGE, transferred onto nitrocellulose membranes and immunoblotted. Primary antibodies recognized Akt (Cell Signaling Technologies, #2920, USA), phospho-T308 Akt (Cell Signaling Technologies, #13038), Akt phospho-S473 Akt (Cell Signaling Technologies, #4060), phospho-T642 Tbc1d4 (Cell Signaling Technologies, #8821), Gapdh (Cell Signaling Technologies, #2118), and GLUT4 (polyclonal antibody recognizing the C-terminus of GLUT4 provided by Professor Geoff Holman and Professor Francoise Koumanov from University of Bath). Membranes were incubated with the appropriate HRP-conjugated or Alexa Fluor-conjugated secondary antibodies for 1—2 h at RT. Protein bands were visualized using ECL (Thermo Fisher Scientific) or 647-fluorescence intensity on the Chemidoc MP (Bio-Rad, USA), and densitometry performed using Image Lab 6.0.1 (Bio-Rad).

2.9. siRNA-mediated knockdown of Picalm in 3T3-L1-cells during differentiation

3T3-L1 fibroblasts (ATTC® CL-173™) were cultured in IMDM (Iscove's Modified Dulbecco's Medium, PAN-Biotech) containing 10 % NBC (newborn calf serum, PAN-Biotech) at 37 °C in 5 % CO_2. Fibro-blasts were seeded on collagen-coated (Collagen A, Biochrom GmbH, Berlin, Germany) cell culture plates. Until cells reached sub-confluence, cells were cultured in IMDM including 10 % FBS (fetal bovine serum, PAN-Biotech) and siRNA treatment was performed. For this, siRNA (Picalm: L-041440-01-0020; non-targeting: D-001810-10-20; Horizon Discovery, Waterbeach, UK) and Lipofectamine RNAi-MAX (Invitrogen) were preincubated and added to the cell culture medium at a final concentration of 60 nM. After two days of incubation, the differentiation was started using an adipogenic cocktail (200 nM insulin (Roche), 0.5 mM 3-isobutyl-1-methylxanthine (Sigma—Aldrich), 2 μM rosiglitazone (Sigma—Aldrich) and 250 nM dexamethasone (Sigma—Aldrich)) for three days. On day 3, a second siRNA treatment

was performed and cells were cultured in IMDM including 10 % FBS and 200 nM insulin for one day, followed by one day in IMDM/FBS, 200 nM insulin and 1% penicillin/streptomycin (P/S). On day 5, the third siRNA treatment was performed and cells were cultured for two days in IMDM/FBS and 1% P/S. Briefly, siRNA treatments were per-formed two days before initiation of differentiation (day −2) in mature adipocytes, three (day +3) and five days (day +5) after initiation of differentiation.

2.10. Quantification of triglyceride levels in 3T3-L1 adipocytes

The triglyceride levels of 3T3-L1 adipocytes were analyzed using the Randox Triglycerides assay (GPO-PAP, TR210) according to the manufacturer's protocol. The cells were suspended in cold homoge-nization buffer and agitated continuously for 5 min. Cells were har-vested, homogenized and incubated at 70 °C for 5 min with continuous shaking, followed by incubation on ice for 5 min. Cell extracts were centrifuged at $16,200 \times g$ for 10 min at 4 °C and the supernatant was used to quantify the triglyceride and protein level.

2.11. miRNA mimic transfection

3T3-L1 fibroblasts were cultured as described before (see 2.9). 50 nM miRNA mimic miR-30c-5p, miR-344-3p, miR-335-5p, miR-186-5p or miR-30b-5p (YM00471185-ADA, YM00470410-ADA, YM00473600-ADA, YM00471598-ADA, YM00471216-ADA, Qiagen) was trans-fected into sub-confluent 3T3-L1 fibroblasts cells using Lipofectamine 2000 transfection reagent (Invitrogen) compared to a scrambled control miRNA (YM00479902-ADA, Qiagen) and cells were incubated at 37 °C, 5% CO_2 for 48 h.

3. RESULTS

3.1. Expression of *Picalm* across models with varying metabolic status

NZO female mice, which are protected from diabetes under stan-dard diet conditions [7,8], show varying susceptibility to diabetes development when fed a diabetogenic diet containing 60 kcal% from fat. Under these conditions, approximately 40% of mice develop a diabetes-like phenotype (DP, diabetes prone), while the remaining mice are protected from hyperglycemia (DR, diabetes resistant) [10]. It has been shown by our group that a liver fat content of more than 10% at the age of 10 weeks can be used as a predictive marker for the diabetes manifestation at a later age [10]. Since these mice are genetically identical, their inherent hetero-geneity in diabetes susceptibility offers an opportunity to investigate the epigenetic signatures determining the T2D risk. Gonadal white adipose tissue (WAT) RNA-seq analysis revealed the adapter protein *Picalm* as a highly regulated gene between DP and DR mice (n = 15/group), with lower mRNA expression in DR mice ($p < 0.001$), which are protected from hyperglycemia (Figure 1A). This significant reduction in *Picalm* gene expression was also confirmed at the protein level (Figure 1A, Supplementary Figure 2A). Similarly, *Picalm* expression was notably lower in adipose tissue of normoglycemic compared to hyperglycemic (BG > 16.6 mmol/l) male NZO mice ($p < 0.05$; Figure 1B). In this cohort, blood glucose levels as well as body weight exhibited a strong trend toward correlating with *Picalm* expression (p = 0.088 and p = 0.071, Figure 1B, Supplementary Figure 1A).

Moreover, the *Picalm* expression was measured throughout the pro-gression from obesity and insulin resistance to hyperglycemia and beta-cell failure in male NZO mice. This was achieved by a specific feeding regimen of initial carbohydrate restriction (HFD-CH) followed by
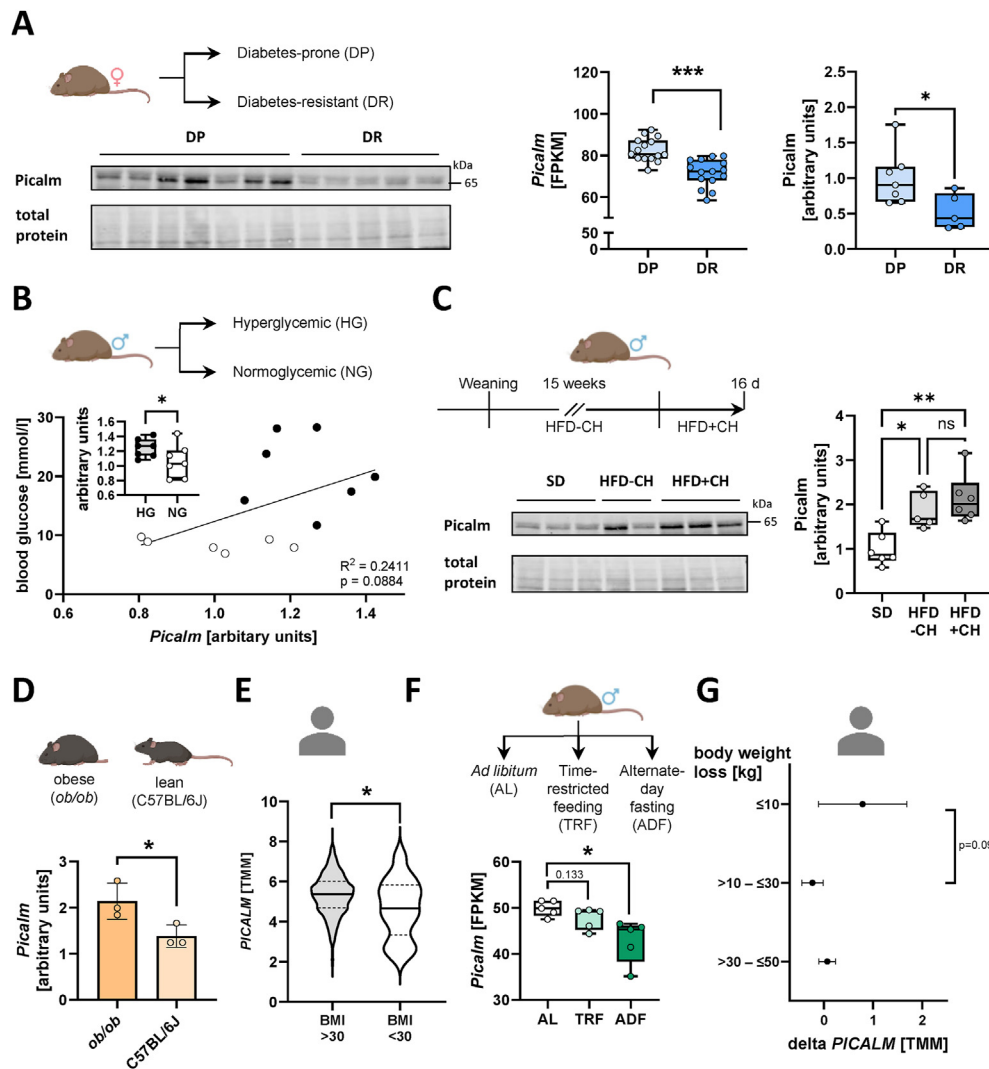
Figure 1: Reduced *Picalm* expression in adipose tissue associates with metabolic health and weight loss in mice and humans. (A) *Picalm* expression in gonadal white adipose tissue (WAT) of diabetes-prone (DP) vs. diabetes-resistant (DR) female NZO mice determined by western blot analysis (right and left panel) and RNA sequencing (middle panel, n = 15/group). (B) WAT Picalm expression in male hyper- and normoglycemic (HG and NG) NZO mice and correlation to blood glucose levels. (C) WAT Picalm expression in NZO males fed a standard diet compared to NZO males fed a carbohydrate-free high-fat diet (HFD-CH) for 15 weeks, inducing obesity and insulin resistance, followed by 16 days of carbohydrate-containing high-fat diet-feeding (HFD+CH), inducing hyperglycemia and beta-cell loss. *p < 0.05, **p < 0.01 by one-way ANOVA. (D) WAT *Picalm* expression of *ob/ob* vs. C57BL/6J mice determined by RT-qPCR (n = 3/group). Bars represent mean ± SEM. *p < 0.05 by one-tailed nonparametric Mann−Whitney test. (E) Human *PICALM* expression in visceral adipose tissue of subjects with obesity (BMI>30, n = 1449) vs. subjects without obesity (BMI<30, n = 31) determined by RNA sequencing. (F) WAT *Picalm* expression (RNA sequencing) of male NZO mice after 5-weeks of time-restricted feeding (TRF, n = 5) or alternate-day fasting (ADF, n = 5) compared to *ad libitum* fed control group (AL; n = 5). (G) Change in human visceral adipose tissue *PICALM* expression (RNA sequencing) after bariatric surgery in subjects with a body weight loss of less than 10 kg (n = 6), between 10 and 30 kg (n = 18) and between 30 and 50 kg (n = 23). *p < 0.05, **p < 0.01 by two-tailed unpaired t-test with Welch correction (D−F). FPKM: Fragments Per Kilobase Million, TMM: Trimmed Mean of M-values. Figures were created, in part, using BioRender.com.

a carbohydrate challenge (HFD+CH) induced glucolipotoxicity in NZO mice, resulting in a synchronized fast beta-cell loss through apoptosis within 16 days. Compared to NZO mice maintained on a standard diet (SD), adipose tissue *Picalm* gene and protein expression was already significantly elevated in obese NZO mice before the switch to carbohydrates (HFD-CH, Figure 1C, Supplementary Figure 1B, 2B,C). Although *Picalm* expression increased further after the introduction of carbohydrates, this increase did not reach statistical significance, and expression levels remained unchanged 16 days after diet switch, indicating that obesity is a major contributor to *Picalm* modulation. Interestingly, the expression of *Picalm* in WAT also varied in other mouse models depending on the obesity status. *Picalm* was expressed at lower levels in WAT of lean C57BL/6J mice compared to obese mice carrying a leptin mutation (C57BL/6J-*ob/ob* mice, p = 0.05, n = 3/group) (Figure 1D). Translation of these findings into humans also revealed a significantly higher *PICALM* expression in visceral adipose tissue (VIS) in individuals with obesity (BMI>30, n = 1449) compared to individuals without (BMI<30, n = 31; p = 0.015; Figure 1E). Among the entire cohort, body fat percentage showed a significant positive correlation with VIS *PICALM* expression (Supplementary Figure 1C). However, the analysis of the protein levels in these samples showed high variability and did not reveal any differences between the two groups nor correlation to the corresponding *PICALM* mRNA levels of each participant (Supplementary Figure 1D−F, 2D,E).
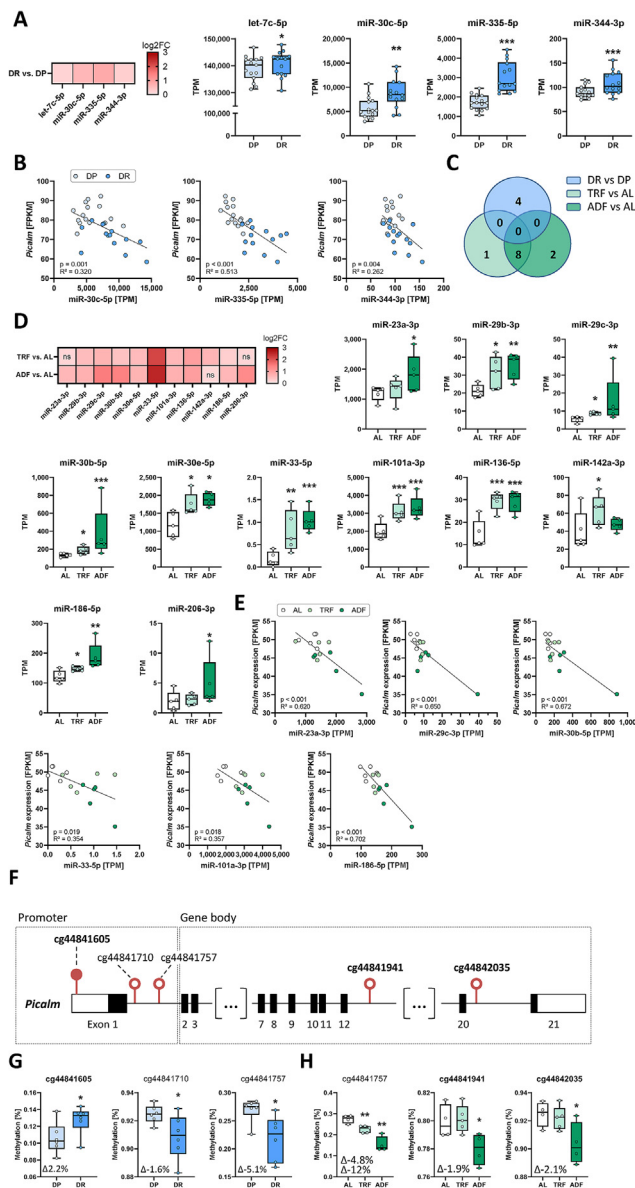
Figure 2: Regulation of adipose tissue *Picalm* expression by miRNAs and DNA methylation. (A) Upregulated *Picalm*-targeting miRNAs in WAT of diabetes-resistant (DR, n = 14) compared to diabetes-prone (DP, n = 15) mice. Heatmap depicts log2FC and box whisker plots indicate median and minimal/maximal miRNA expression values. (B) Linear regression of miRNA and *Picalm* expression in WAT of DP (light blue) and DR (dark blue) mice. (C) Overlap of *Picalm*-targeting miRNAs which are upregulated in WAT of DR compared to DP mice and in WAT of time-restricted feeding (TRF, n = 5) or alternate-day fasting (ADF, n = 5) compared to *ad libitum* fed mice (AL, n = 5). (D) Expression pattern of *Picalm*-targeting miRNAs which are significantly upregulated in TRF and/or ADF compared to AL (indicated by asterisks) and (E) linear regression between miRNA and *Picalm* expression. TPM: Transcripts Per Million. (F) Schematic representation of the murine *Picalm* gene structure, definition of promoter and gene body region and localization of differentially methylated positions. Open circles depict hypomethylated sites and full circles indicate hypermethylated sites. DMP-IDs in bold indicate differentially methylated positions that potentially contribute to downregulation of *Picalm* expression based on the expected associations between methylation in promoter and gene body regions to the gene expression. (G) Methylation levels and delta methylation values of *Picalm* DMPs in DR vs. DP mice and (H) TRF and ADF vs. AL mice asterisks indicate significant differences compared to AL. *$p < 0.05$, **$p < 0.01$, ***$p < 0.001$.

These results raised the question of an association between weight loss and reduced expression of *Picalm*. In diabetes-prone male NZO mice, time-restricted feeding (TRF) and alternate-day fasting (ADF) of a high-fat diet are sufficient to prevent hyperglycemia [5,6]. *Picalm* gene expression in WAT decreased significantly after 5 weeks of ADF ($p < 0.001$) and exhibited an intermediate pattern with the less strict TRF intervention ($p = 0.133$, n = 5/group) (Figure 1F), an effect that showed a similar trend at the protein level in WAT (Supplementary Figure 1G, 2F). In order to test if *PICALM* gene expression is also affected by body weight loss in humans, we evaluated its expression in VIS biopsies of subjects with morbid obesity before and after bariatric surgery, i.e. in relation to the achieved body weight loss. Similar to the effects seen in mice, *PICALM* expression after surgery tended to be lower in individuals who lost more than 10 kg body weight (n = 41) compared to those that lost less than 10 kg (n = 6) (Figure 1G).

Given the link between Picalm expression and adiposity, we suspected a possible association with adipogenic and inflammatory processes. Upon screening of the transcriptome data from DP and DR as well as AL, TRF and ADF mice, we indeed found a significant correlation of WAT *Picalm* levels with genes involved in fat cell differentiation and insulin stimulus, including GLUT4 (*Slc2a4*), as well as multiple inflammatory markers (Supplementary Figure 3A,B). In the human cross-sectional cohort, IL6 levels significantly correlated with VIS *PICALM* expression, but no correlation was found to CRP levels (Supplementary Figure 3C).

3.2. Epigenetic mechanisms regulating *Picalm* expression in adipose tissue

As the expression of *Picalm* was associated with diabetes susceptibility in genetically identical mice and dietary restriction was sufficient to downregulate the levels of *Picalm*, we were interested if common epigenetic mechanisms contribute to the regulation of murine *Picalm* expression in the context of diabetes predisposition (DP vs. DR) and dietary protection from diabetes (TRF, ADF vs. AL). Screening for differentially expressed miRNAs in WAT targeting *Picalm* revealed four candidates: let-7c-5p, miR-30c-5p, miR-335-5p, and miR-344-3p, which were higher expressed in WAT of DR compared to DP mice, with log2FC values ranging from 0.19 to 0.83 (Figure 2A). Except for let-7c-5p, the WAT expression of all other miRNAs significantly correlated with *Picalm* expression in adipose tissue, suggesting that these miRNAs may contribute to the downregulation of *Picalm* expression observed in DR mice (Figure 2B). Among these, miR-30c-5p exhibited the highest level of expression and the second highest log2FC of 0.83 (Figure 2A), implying that it may be the most relevant for *Picalm* suppression. Interestingly, none of these miRNAs were significantly regulated by the two dietary interventions (TRF or ADF) in WAT of NZO mice (Figure 2C), although miR-355-5p exhibited a strong trend towards upregulation following ADF ($p = 0.052$, Supplementary Figure 4A). Of note, *Picalm*-targeting miR-30a-5p was higher expressed in both DR and ADF, however, this did not reach statistical significance ($p < 0.1$, Supplementary Figure 4B). In fact, 11 other *Picalm*-targeting miRNAs were TRF and/or ADF-responsive (Figure 2D). Compared to DP vs. DR, significantly higher log2FC values were observed, particularly in the more stringent ADF intervention. As shown in Figure 2D, miR-33-5p exhibited the highest log2FC in both TRF (log2FC = 2.17) and ADF (log2FC = 2.55) compared to AL, although with a generally low expression overall. Nevertheless, its expression significantly correlated with *Picalm* expression (Figure 2E). Out of the 11 regulated miRNAs targeting
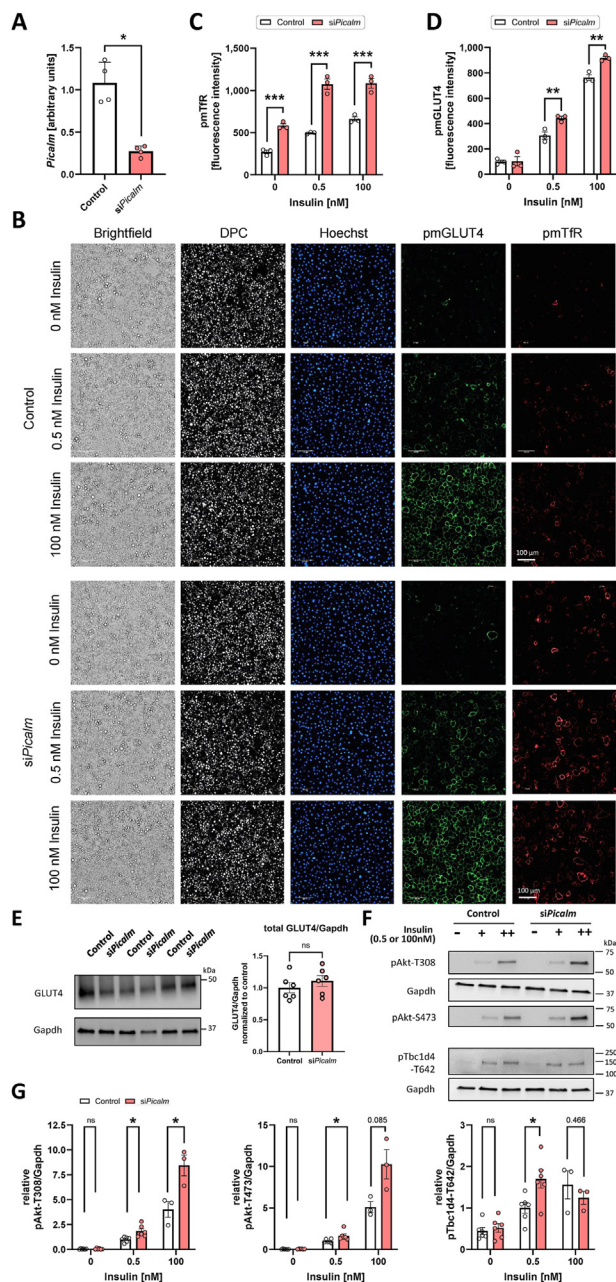
Picalm, 6 correlated with *Picalm* expression, including the highly abundant miRNAs, miR-101a-3p, miR-23a-3p, and miR-30b-5p.

To investigate the direct relationship between altered miRNA expression and reduced *Picalm* mRNA levels, functional assays were conducted in 3T3-L1 fibroblasts. The fibroblasts were treated with miRNA mimics, and *Picalm* expression was analyzed 48 h after transfection (Supplementary Figure 4C). For these studies, a subset of significantly altered miRNAs was selected based on their correlation with *Picalm* expression and fold change between the compared groups. As illustrated in Supplementary Figure 4D, with the exception of miR-30c-5p, transfection with the selected mimics resulted in elevated levels of the respective miRNA 48 h post-treatment. However, the overexpression of miR-344-3p, miR-186-5p and miR-30c-5p only slightly reduced *Picalm* levels, but this reduction did not reach statistical significance (Supplementary Figure 4E). Nonetheless, additional experiments are required, particularly those involving the combination of different miRNAs, to draw definitive conclusions whether the expression of *Picalm* is influenced by the level of specific miRNAs targeting *Picalm* in adipose tissue.

Next, we explored changes in DNA methylation that might contribute to *Picalm* regulation. In DP vs. DR mice, three differentially methylated CpG positions (DMP) were identified in the promoter region of the *Picalm* gene, including the first intron (Figure 2F). Higher methylation levels of cytosines within the promoter region, often also including the first intron, are generally associated with reduced gene expression. One DMP in the promoter region showed a significantly higher level of methylation in DR compared to DP mice (hypermethylation) aligning with reduced *Picalm* expression, although the difference in methylation was only 2.2% (Figure 2G). The strongest methylation difference in DR as well as in TRF and ADF groups was observed for the DMP cg44841757, which localizes in the first intron and was hypomethylated in all groups (Figure 2G). However, assuming that hypomethylation in the promoter region (including first intron) is linked to an increase in gene expression, this change cannot account for reduced expression of *Picalm* in adipose tissue. Opposite to the promoter region, hypomethylation in the gene body generally associates with lower gene expression. In response to ADF, two additional gene body DMPs were hypomethylated, although again with low delta methylation of around 2% (Figure 2H), suggesting that these DMPs might participate in fine-tuning *Picalm* downregulation. Overall, DNA methylation seems to play a minor role in *Picalm* regulation in the mouse models that we investigated.

3.3. Impact of Picalm on adipocyte GLUT4 trafficking

As a clathrin-adapter protein, Picalm plays a critical role in clathrin-mediated endocytosis and multiple studies have reported that Picalm depletion causes differences in transferrin uptake [27–31]. However, these effects appear to be cell-type specific, since studies in other systems did not report alterations in transferrin trafficking [32,33]. To our knowledge, no studies on the function of *Picalm* have been performed in adipocytes or adipose tissue. The involvement of Picalm in cellular transport processes, along with our new findings that the expression pattern varies depending on body weight, suggest that it also plays a role in processes regulating insulin sensitivity and responses, for example insulin-regulated GLUT4-translocation in adipocytes. Therefore, we employed a previously established imaging-based assay to assess endogenous GLUT4-translocation in 3T3-L1 adipocytes treated with a non-targeting siRNA (control), or siRNA targeting *Picalm* (si*Picalm*) [26]. In brief, the use of a recently developed antibody targeting the exofacial domain of GLUT4 [34] allowed
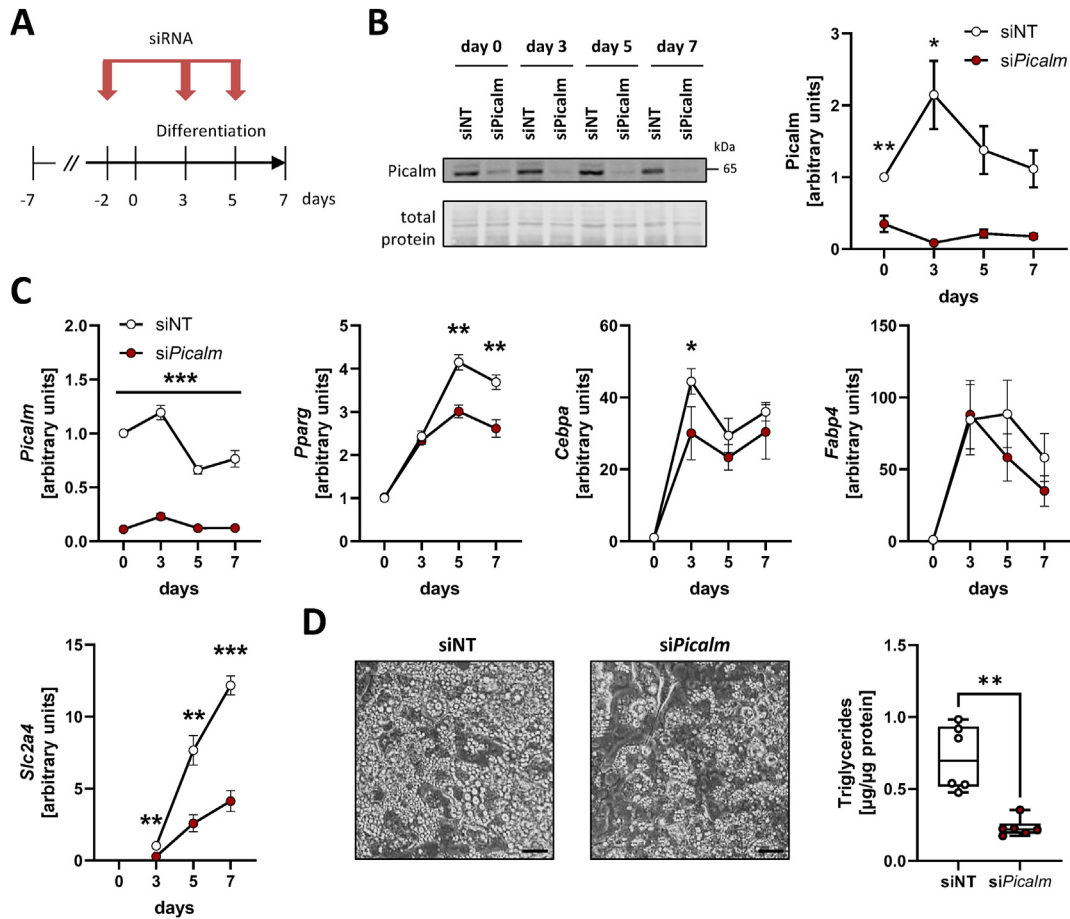
Figure 3: *Picalm* **knockdown in 3T3-L1 cells increase insulin-stimulated GLUT4-translocation**. (A) 3T3-L1 adipocytes were treated with siRNA targeting *Picalm* or with non-targeting siRNA (control). Results of *Picalm* RT-qPCR verified a successful knockdown. **p < 0.01 by two-tailed unpaired t-test with Welch correction. (B) 3T3-L1 adipocytes were stimulated with 0, 0.5 or 100 nM insulin for 20 min and subsequently, non-permeabilized cells were stained for plasma membrane GLUT4 (pmGLUT4) and plasma membrane transferrin receptor (pmTfR). Presented are representative pictures of brightfield, digital phase contrast (DPC), and confocal images. (C) Quantification of pmTfR levels at indicated insulin levels and (D) quantification of pmGLUT4 shown for control and si*Picalm* cells. (E) Western blot analysis of total GLUT4 in control and si*Picalm* 3T3-L1 cells normalized to Gapdh. ns: not significant by unpaired t-test with Welch correction. (F) Representative images and (G) quantification of western blot analysis of Akt and Tbc1d4 phosphorylation in 3T3-L1 cells with and without *Picalm* knockdown under basal conditions and after insulin stimulation (0.5 nM (+) or 100 nM (++) for 20 min). Relative values are shown, normalized to the mean of control cells treated with 0.5 nM insulin. Data represent mean ± SEM. *p < 0.05, **p < 0.01, ***p < 0.001 by two-way ANOVA with Sidak's multiple comparison test (C,D) or unpaired t-test with Welch correction (F).

Figure 4: Picalm depletion attenuates 3T3-L1 adipogenesis. (A) Experimental design: sub-confluent 3T3-L1 fibroblasts were treated with siRNA two days before, and on days 3 and 5 after start of differentiation. (B) Picalm expression in Picalm-knockdown (si*Picalm*) and non-targeting siRNA-treated (siNT) 3T3-L1 cells during differentiation. (C) *Picalm* and adipogenesis marker gene expression in si*Picalm* compared to siNT cells, determined by qRT-PCR. (D) Representative pictures of 3T3-L1 adipocytes with and without Picalm-knockdown after 7 days of differentiation (left panel) and quantification of triglyceride levels on day 7. *$p < 0.05$, **$p < 0.01$, ***$p < 0.001$ by two-way ANOVA with Sidaks correction (B—C) or unpaired t-test with Welch correction (D). Data represent the mean $\pm$ SEM of two independent experiments, each performed with three replicates per group.

the detection and quantification of transport-competent GLUT4 at the plasma membrane of non-permeabilized cells. Using a specific siRNA targeting *Picalm*, the expression was downregulated by over 70% (Figure 3A). As a control for Picalm depletion impairing clathrin-mediated endocytosis, we assessed plasma membrane transferrin receptor (pmTfR) levels in unstimulated and insulin-stimulated adipocytes. As previously reported [26], insulin increased pmTfR content in control cells dose-dependently. Depletion of *Picalm* had a pronounced effect on pmTfR levels in both the absence and presence of insulin (Figure 3B,C).

Insulin dose-dependently increased endogenous GLUT4 at the plasma membrane (pmGLUT4), but this increase was significantly enhanced in *Picalm* knockdown adipocytes in response to both 0.5 nM and 100 nM insulin (Figure 3B,D). The quantification of total cellular GLUT4 by western blot showed no differences between control and si*Picalm* cells, confirming that *Picalm* depletion amplifies surface GLUT4 by altered trafficking responses (Figure 3E, Supplementary Figure 5A).

GLUT4-trafficking from intracellular compartments (GSVs, GLUT4-storage vesicles) to the plasma membrane is enhanced by activation of the PI3K/Akt signaling pathway downstream of the insulin receptor [35]. Therefore, we investigated whether insulin signaling is also affected following *Picalm* knockdown and if this alteration could

account for the increased GLUT4-translocation in 3T3-L1 cells. The phosphorylation of Akt was analyzed under basal and insulin-stimulated (0.5 nM; 100 nM) conditions in 3T3-L1 adipocytes after siRNA-mediated downregulation of *Picalm*. We measured significantly higher insulin-stimulated Akt phosphorylation at T308 and S473 in *Picalm* knockdown cells compared to cells treated with non-targeting siRNA at both 0.5 nM and 100 nM, respectively (Figure 3F,G, Supplementary Figure 5B,C). Activated Akt phosphorylates the Rab GTPase-activating protein Tbc1d4/AS160, primarily at T642, which then allows GSVs to move to and fuse with the plasma membrane [36]. In our study, 3T3-L1 cells with reduced *Picalm* expression exhibited a significant increase in insulin-stimulated phosphorylation of Tbc1d4 in comparison to cells treated with control siRNA at 0.5 nM insulin, but not at 100 nM (Figure 3F,G, Supplementary Figure 5B,C). These findings suggest that Picalm depletion leads to an amplification of proximal insulin signaling to Akt in adipocytes, but this is not passed to downstream substrates at higher insulin doses. As such, the effect of Picalm-knockdown on pmGLUT4 at 100 nM may be due to direct effects on GLUT4 trafficking. In conclusion, a downregulation of *Picalm* in adipocytes, as observed in response to beneficial life-style interventions and in DR mice (Figure 1), enhances insulin-stimulated translocation of GLUT4 to the cell surface.

3.4. Role of Picalm on adipogenesis

Given the importance of insulin action on adipogenesis, the effects of altered Picalm levels on differentiation of 3T3-L1 cells were tested. First, endogenous Picalm levels during differentiation in 3T3-L1 cells were analyzed. While *Picalm* mRNA was high in premature adipocytes and lower in mature adipocytes, the protein levels were markedly increased during adipogenesis, reaching a maximum at 5 days after start of differentiation and then decreasing until the final day 7 of differentiation (Supplementary Figure 6A,B). These data imply that Picalm may play a role in the early stages of differentiation. Consequently, siRNA-mediated knockdown was carried out prior to the onset and throughout differentiation to achieve effective suppression of Picalm expression (Figure 4A,B, Supplementary Figure 7A-F). The expression of *Pparg*, one of the key adipogenic regulators failed to increase to the same extent as observed in cells treated with non-targeting siRNA, leading to significantly lower levels in Picalm-knockdown cells on day 5 and 7 (Figure 4C). A similar pattern was observed for the adipogenic marker genes *Cepba* and *Fabp4* (Figure 4C). Most strikingly, the increase in GLUT4 (*Slc2a4*) expression during adipogenesis was significantly diminished in Picalm-knockdown cells (Figure 4C). In untreated 3T3-L1 cells, *Slc2a4* levels increased over 10-fold by the end of differentiation, whereas in si*Picalm* cells, the expression of the glucose transporter reached only about 4-fold. Finally, quantification of cell triglyceride levels at day 7 of differentiation indicated that Picalm-depleted 3T3-L1 adipocytes stored significantly less neutral lipids (Figure 4D), confirming a severe adipogenesis defect. In conclusion, these data provide direct functional evidence that Picalm is involved in regulating the differentiation in adipocytes.

4. DISCUSSION

The adapter protein Picalm (phosphatidylinositol binding clathrin assembly protein) plays a crucial role in clathrin-mediated endocytosis, a process essential for the internalization of various receptors and transporters, and polymorphisms within the gene are associated with the risk of Alzheimer's disease [9]. The current study investigates the expression, regulation and functional impact of Picalm in adipose tissue. In white adipose tissue, reduced *Picalm* expression was associated with a lower diabetes risk and body weight in mice and humans, potentially due to an altered expression of specific miRNAs targeting *Picalm*. Beyond this, our data showed that Picalm affects both GLUT4-translocation and insulin signaling as demonstrated by increased insulin-stimulated surface GLUT4, pAkt, and pTbc1d4 after knockdown in mature 3T3-L1 adipocytes, highlighting the role of Picalm in maintaining metabolic health and insulin sensitivity. Although we initially hypothesized enhanced adipogenesis when depleting Picalm before and during differentiation, expecting increased insulin action, we instead observed significant defects in adipogenesis. This suggests that Picalm regulates various aspects of adipocyte biology and may have distinct roles in preadipocytes and mature fat cells.

Although adipose tissue expression of *Picalm* was altered in NZO female mice based on their susceptibility to diabetes and also in NZO males in response to caloric restriction, no common pattern of epigenetic regulation was identified on the level of miRNA's and DNA methylation. Moreover, our data indicate that post-transcriptional repression by miRNAs is more relevant for *Picalm* regulation under various metabolic conditions than regulation by methylation changes. First results indicate that miR-344-3p and miR-30b-5p might partially account for reduced Picalm levels in WAT, although experiments using a combination of multiple miRNAs at once might provide more conclusive insights into the significance of miRNAs in regulating the expression of Picalm.

The miRNA-specific regulation of *Picalm* expression has already been documented. Recent studies in hepatocytes have provided evidence that the miR-155-5p binds to the 3′-UTR of *Picalm* mRNA leading to reduced expression levels [37] and also exosomal miR-155 was shown to act as virus inhibitor, suppressing EV-A71 infection through targeting *Picalm in vitro* and *in vivo* [38]. In the context of Alzheimer's disease, numerous miRNAs (such as miR-142 [39] and miR-153 [40]) have been shown to target *Picalm*, however, none of these described miRNAs were changed in our models. These findings underscore the tissue-specific regulation of *Picalm* by miRNAs, suggesting that the effects of miRNAs on Picalm can vary depending on the cellular context and the presence of specific regulatory mechanisms within different tissues. This tissue-specific regulation seems to be critical for understanding the diverse roles of Picalm in health and disease [9].

Studies linking *Picalm* to glucose homeostasis are limited. Chae et al. focused on the link between diabetes and Alzheimer's disease [41]. In human neuroblastoma cells high glucose-induced early endosomal abnormalities through PICALM-induced amyloid precursor protein endocytosis and mTORC1-inhibited endosomal clearance, upregulating amyloid β production. Thus, the authors postulate that targeting PICALM represents a promising approach for managing diabetes-induced Alzheimer's disease by preventing endosomal disorders. Another study also demonstrates an association between a SNP within the PICALM gene and gestational diabetes as well as impaired glucose tolerance [42]. These distinct functions of PICALM are probably achieved by specific trafficking and/or signaling in different cell types.

GLUT4 is the most abundant glucose transporter in adipocytes and recycles between the plasma membrane and intracellular storage vesicles [3]. Its steady-state distribution is regulated through insulin-dependent signaling cascades that involve the Akt kinase and its substrate RabGAP protein Tbc1d4 [3]. Our results indicate that Picalm depletion amplifies insulin-induced pmGLUT4 through enhanced activation of the GLUT4 branch of insulin signaling, as evidenced by increased Akt and Tbc1d4 phosphorylation. It is worth noting that recent screens for regulators of GLUT4-trafficking in 3T3-L1 cells have almost exclusively identified genes whose absence led to a reduction in translocation [26,43]. This makes Picalm especially interesting as a potential drug target.

One possible explanation for the cause of increased insulin signaling after Picalm knockdown in 3T3-L1 cells could be a delay in insulin receptor internalization. Since the insulin receptor is internalized via clathrin-mediated endocytosis, it appears likely that Picalm depletion could interfere with this process and thereby prolong the activation of downstream insulin signaling. Experiments focusing on the abundance of the insulin receptor at the cell surface in settings equivalent to the GLUT4 and TfR-assay presented in this paper could eventually contribute to define how Picalm modules insulin signaling. Additionally, it is plausible that loss of Picalm also directly delays GLUT4 recycling since we observed no increase in Tbc1d4 phosphorylation at 100 nM insulin, despite increased Akt phosphorylation at this dose. At 100 nM insulin, the signaling pathway controlling GLUT4-translocation is fully activated [44], and therefore the increase in GLUT4-translocation with Picalm-knockdown may be attributed to slower GLUT4 internalization.

The involvement of Picalm in clathrin-mediated endocytosis is well studied. However, the effects of *Picalm* depletion on transferrin uptake, which is a commonly used method to assess efficiency of clathrin-mediated endocytosis, vary depending on the cell type under test [27,31—33]. We found that *Picalm* knockdown majorly enhanced TfR

abundance at the plasma membrane in 3T3-L1 adipocytes, suggesting decreased clathrin-mediated endocytosis. Increased surface TfR was observed in absence and presence of insulin, while surface GLUT4 was only enhanced after insulin stimulation. This may be explained by the dominance of distinct internalization routes for GLUT4 under basal and insulin-stimulated conditions; whereas TfR endocytosis generally depends on clathrin, GLUT4 is internalized via clathrin-dependent and -independent routes. In unstimulated adipocytes, around 80% of GLUT4 internalization was shown to occur nystatin-sensitive and independent of clathrin [45], which may explain why we only observed increased pmGLUT4 under insulin-stimulated conditions when GLUT4 is predominantly internalized via clathrin-mediated pathways [45].

A distinct function of Picalm, which sets it apart from other clathrin-adapter proteins, is its ability to directly bind the small R-SNARE proteins VAMP2, VAMP3, and VAMP8, facilitating their endocytosis [46]. VAMP8 has been shown to mediate GLUT4 endocytosis [47], which suggests that Picalm might act as a specific adapter for GLUT4 recycling.

Besides Picalm's role in modulating insulin signaling, the study also demonstrated that Picalm directly affects adipogenesis. Considering that insulin signaling is a critical component of adipogenesis, the reduced differentiation capacity of Picalm-depleted cells rather hints towards a more nuanced role of Picalm in different stages of adipocyte maturation that might go beyond alterations in insulin signaling.

5. CONCLUSION

In summary, our study revealed that reduced Picalm expression in adipose tissue in both mice and humans is linked to beneficial health outcomes, including weight loss and diabetes prevention. Our experiments conclusively showed that Picalm plays a role in insulin responses and GLUT4-translocation in adipocytes. Further research is needed to determine whether this effect is solely due to amplified insulin signaling or if specific trafficking events also play a role. Finally, we propose that reduced *Picalm* expression in adipose tissue may play a functional role in enhancing insulin sensitivity.

CREDIT AUTHORSHIP CONTRIBUTION STATEMENT

Jasmin Gaugel: Writing — review & editing, Writing — original draft, Visualization, Methodology, Investigation, Formal analysis, Conceptualization. **Neele Haacke:** Methodology, Formal analysis. **Ratika Sehgal:** Methodology, Formal analysis, Data curation. **Markus Jähnert:** Methodology, Formal analysis, Data curation. **Wenke Jonas:** Data curation. **Anne Hoffmann:** Methodology, Formal analysis, Data curation. **Matthias Blüher:** Resources, Funding acquisition, Data curation, Conceptualization. **Adhideb Ghosh:** Methodology, Formal analysis, Data curation. **Falko Noé:** Methodology, Formal analysis. **Christian Wolfrum:** Resources, Data curation. **Joycelyn Tan:** Investigation, Formal analysis. **Annette Schürmann:** Supervision, Resources, Funding acquisition. **Daniel J. Fazakerley:** Writing — review & editing, Supervision, Resources, Investigation, Funding acquisition, Formal analysis. **Heike Vogel:** Writing — review & editing, Supervision, Methodology, Funding acquisition, Conceptualization.

DECLARATION OF COMPETING INTEREST

MB received honoraria as a consultant and speaker from Amgen, AstraZeneca, Bayer, Boehringer-Ingelheim, Lilly, Novo Nordisk, Novartis, and Sanofi. All other authors declare no conflicts of interest. The funders had no role in the design of the study; in the collection, analyses, or interpretation of data; in the writing of the manuscript; or in the decision to publish the results. All other authors declare that there are no conflicts of interests.

DATA AVAILABILITY

Data will be made available on request.

APPENDIX A. SUPPLEMENTARY DATA

Supplementary data to this article can be found online at https://doi.org/10.1016/j.molmet.2024.102014.

REFERENCES

[1] Ng JM, Azuma K, Kelley C, Pencek R, Radikova Z, Laymon C, et al. PET imaging reveals distinctive roles for different regional adipose tissue depots in systemic glucose metabolism in nonobese humans. Am J Physiol Endocrinol Metab 2012;303(9). https://doi.org/10.1152/ajpendo.00282.2012.

[2] Fazakerley DJ, Krycer JR, Kearney AL, Hocking SL, James DE. Muscle and adipose tissue insulin resistance: malady without mechanism? J Lipid Res 2019;60(10):1720—32. https://doi.org/10.1194/jlr.R087510.

[3] Chadt A, Al-Hasani H. Glucose transporters in adipose tissue, liver, and skeletal muscle in metabolic health and disease. Pflug Arch Eur J Physiol 2020;472(9):1273—98. https://doi.org/10.1007/s00424-020-02417-x.

[4] Kleinert M, Clemmensen C, Hofmann SM, Moore MC, Renner S, Woods SC, et al. Animal models of obesity and diabetes mellitus. Nat Rev Endocrinol 2018;14(3):140—62. https://doi.org/10.1038/nrendo.2017.161.

[5] Baumeier C, Kaiser D, Heeren J, Scheja L, John C, Weise C, et al. Caloric restriction and intermittent fasting alter hepatic lipid droplet proteome and diacylglycerol species and prevent diabetes in NZO mice. Biochim Biophys Acta Mol Cell Biol Lipids 2015;1851(5):566—76. https://doi.org/10.1016/j.bbalip.2015.01.013.

[6] Quiclet C, Dittberner N, Gässler A, Stadion M, Gerst F, Helms A, et al. Pancreatic adipocytes mediate hypersecretion of insulin in diabetes-

susceptible mice. Metab Clin Exp 2019. https://doi.org/10.1016/j.metabol.2019.05.005.

[7] Ortlepp JR, Kluge R, Giesen K, Plum L, Radke P, Hanrath P, et al. A metabolic syndrome of hypertension, hyperinsulinaemia and hypercholesterolaemia in the New Zealand obese mouse. Eur J Clin Investig 2000;30(3):195—202. https://doi.org/10.1046/j.1365-2362.2000.00611.x.

[8] Vogel H, Mirhashemi F, Liehl B, Taugner F, Kluth O, Kluge R, et al. Estrogen deficiency aggravates insulin resistance and induces β-cell loss and diabetes in female New Zealand obese mice. Horm Metab Res 2013;45(6):430—5. https://doi.org/10.1055/s-0032-1331700.

[9] Ando K, Nagaraj S, Küçükali F, de Fisenne MA, Kosa AC, Doeraene E, et al. PICALM and Alzheimer's disease: an update and perspectives. Cells 2022;11(24). https://doi.org/10.3390/cells11243994.

[10] Lubura M, Hesse D, Kraemer M, Hallahan N, Schupp M, von Löffelholz C, et al. Diabetes prevalence in NZO females depends on estrogen action on liver fat content. Am J Physiol Endocrinol Metab 2015;309(12):E968—80. https://doi.org/10.1152/ajpendo.00338.2015.

[11] Ouni M, Eichelmann F, Jähnert M, Krause C, Saussenthaler S, Ott C, et al. Differences in DNA methylation of HAMP in blood cells predicts the development of type 2 diabetes. Mol Metab 2023;75(July):101774. https://doi.org/10.1016/j.molmet.2023.101774.

[12] Ouni M, Schürmann A. Epigenetic contribution to obesity. Mamm Genome 2020;31(5—6):134—45. https://doi.org/10.1007/s00335-020-09835-3.

[13] Kluth O, Matzke D, Schulze G, Schwenk RW, Joost HG, Schürmann A. Differential transcriptome analysis of diabetes-resistant and -sensitive mouse islets reveals significant overlap with human diabetes susceptibility genes. Diabetes 2014;63(12):4230—8. https://doi.org/10.2337/db14-0425.

[14] Mulhem A, Moulla Y, Klöting N, Ebert T, Tönjes A, Fasshauer M, et al. Circulating cell adhesion molecules in metabolically healthy obesity. Int J Obes 2021;45(2):331—6. https://doi.org/10.1038/s41366-020-00667-4.

[15] Dobin A, Davis CA, Schlesinger F, Drenkow J, Zaleski C, Jha S, et al. STAR: ultrafast universal RNA-seq aligner. Bioinformatics 2013;29(1):15—21. https://doi.org/10.1093/bioinformatics/bts635.

[16] Love MI, Huber W, Anders S. Moderated estimation of fold change and dispersion for RNA-seq data with DESeq2. Genome Biol 2014;15(12):1—21. https://doi.org/10.1186/s13059-014-0550-8.

[17] Picelli S, Faridani OR, Björklund ÅK, Winberg G, Sagasser S, Sandberg R. Full-length RNA-seq from single cells using Smart-seq2. Nat Protoc 2014;9(1):171—81. https://doi.org/10.1038/nprot.2014.006.

[18] Song Y, Milon B, Ott S, Zhao X, Sadzewicz L, Shetty A, et al. A comparative analysis of library prep approaches for sequencing low input translatome samples. BMC Genom 2018;19(1):1—16. https://doi.org/10.1186/s12864-018-5066-2.

[19] Kozomara A, Birgaoanu M, Griffiths-Jones S. MiRBase: from microRNA sequences to function. Nucleic Acids Res 2019;47(D1):D155—62. https://doi.org/10.1093/nar/gky1141.

[20] Huang HY, Lin YCD, Li J, Huang KY, Shrestha S, Hong HC, et al. MiRTarBase 2020: updates to the experimentally validated microRNA-target interaction database. Nucleic Acids Res 2020;48(D1):D148—54. https://doi.org/10.1093/nar/gkz896.

[21] Karagkouni D, Paraskevopoulou MD, Chatzopoulos S, Vlachos IS, Tastsoglou S, Kanellos I, et al. DIANA-TarBase v8: a decade-long collection of experimentally supported miRNA-gene interactions. Nucleic Acids Res 2018;46(D1):D239—45. https://doi.org/10.1093/nar/gkx1141.

[22] Xiao F, Zuo Z, Cai G, Kang S, Gao X, Li T. miRecords: an integrated resource for microRNA-target interactions. Nucleic Acids Res 2009;37(Suppl. 1):105—10. https://doi.org/10.1093/nar/gkn851.

[23] Zhou W, Triche TJ, Laird PW, Shen H. SeSAMe: reducing artifactual detection of DNA methylation by Infinium BeadChips in genomic deletions. Nucleic Acids Res 2018;46(20):1—15. https://doi.org/10.1093/nar/gky691.

[24] Zhou W, Hinoue T, Barnes B, Mitchell O, Iqbal W, Lee SM, et al. DNA methylation dynamics and dysregulation delineated by high-throughput profiling in the mouse. Cell Genom 2022;2(7). https://doi.org/10.1016/j.xgen.2022.100144.

[25] Ritchie ME, Phipson B, Wu D, Hu Y, Law CW, Shi W, et al. Limma powers differential expression analyses for RNA-sequencing and microarray studies. Nucleic Acids Res 2015;43(7):e47. https://doi.org/10.1093/nar/gkv007.

[26] Diaz-Vegas A, Norris DM, Jall-Rogg S, Cooke KC, Conway OJ, Shun-Shion AS, et al. A high-content endogenous GLUT4 trafficking assay reveals new aspects of adipocyte biology. Life Sci Alliance 2023;6(1):1—19. https://doi.org/10.26508/lsa.202201585.

[27] Ishikawa Y, Maeda M, Pasham M, Aguet F, Tacheva-Grigorova SK, Masuda T, et al. Role of the clathrin adaptor PICALM in normal hematopoiesis and polycythemia vera pathophysiology. Haematologica 2015;100(4):439—51. https://doi.org/10.3324/haematol.2014.119537.

[28] Moreau K, Fleming A, Imarisio S, Lopez Ramirez A, Mercer JL, Jimenez-Sanchez M, et al. PICALM modulates autophagy activity and tau accumulation. Nat Commun 2014;5. https://doi.org/10.1038/ncomms5998.

[29] Dreyling MH, Martinez-Climent JA, Zheng M, Mao J, Rowley JD, Bohlander SK. The t(10;11)(p13;q14) in the U937 cell line results in the fusion of the AF10 gene and CALM, encoding a new member of the AP-3 clathrin assembly protein family. Proc Natl Acad Sci U S A 1996;93(10):4804—9. https://doi.org/10.1073/pnas.93.10.4804.

[30] Klebig ML, Wall MD, Potter MD, Rowe EL, Carpenter DA, Rinchik EM. Mutations in the clathrin-assembly gene Picalm are responsible for the hematopoietic and iron metabolism abnormalities in fit1 mice. Proc Natl Acad Sci U S A 2003;100(14):8360—5. https://doi.org/10.1073/pnas.1432634100.

[31] Suzuki M, Tanaka H, Tanimura A, Tanabe K, Oe N, Rai S, et al. The clathrin assembly protein PICALM is required for erythroid maturation and transferrin internalization in mice. PLoS One 2012;7(2). https://doi.org/10.1371/journal.pone.0031854.

[32] Huang F, Khvorova A, Marshall W, Sorkin A. Analysis of clathrin-mediated endocytosis of epidermal growth factor receptor by RNA interference. J Biol Chem 2004;279(16):16657—61. https://doi.org/10.1074/jbc.C400046200.

[33] Harel A, Wu F, Mattson MP, Morris CM, Yao PJ. Evidence for CALM in directing VAMP2 trafficking. Traffic 2008;9(3):417—29. https://doi.org/10.1111/j.1600-0854.2007.00694.x.

[34] Tucker DF, Sullivan JT, Mattia KA, Fisher CR, Barnes T, Mabila MN, et al. Isolation of state-dependent monoclonal antibodies against the 12-transmembrane domain glucose transporter 4 using virus-like particles. Proc Natl Acad Sci U S A 2018;115(22):E4990—9. https://doi.org/10.1073/pnas.1716788115.

[35] van Gerwen J, Shun-Shion AS, Fazakerley DJ. Insulin signalling and GLUT4 trafficking in insulin resistance. Biochem Soc Trans 2023;51(3):1057—69. https://doi.org/10.1042/BST20221066.

[36] Sakamoto K, Holman GD. Emerging role for AS160/TBC1D4 and TBC1D1 in the regulation of GLUT4 traffic. Am J Physiol Endocrinol Metab 2008;295(1). https://doi.org/10.1152/ajpendo.90331.2008.

[37] Chen X, Lu T, Zheng Y, Lin Z, Liu C, Yuan D, et al. miR-155-5p promotes hepatic steatosis via PICALM-mediated autophagy in aging hepatocytes. Arch Gerontol Geriatr 2024;120(December 2023):105327. https://doi.org/10.1016/j.archger.2024.105327.

[38] Wu J, Gu J, Shen L, Fang D, Zou X, Cao Y, et al. Exosomal microrna-155 inhibits enterovirus a71 infection by targeting picalm. Int J Biol Sci 2019;15(13):2925—35. https://doi.org/10.7150/ijbs.36388.

[39] Ghanbari M, Munshi ST, Ma B, Lendemeijer B, Bansal S, Adams HH, et al. A functional variant in the miR-142 promoter modulating its expression and conferring risk of Alzheimer disease. Hum Mutat 2019;40(11):2131—45. https://doi.org/10.1002/humu.23872.

[40] Amber S, Zahid S. An in silico approach to identify potential downstream targets of miR-153 involved in Alzheimer's disease. Front Genet 2024;15(January):1—9. https://doi.org/10.3389/fgene.2024.1271404.

[41] Chae CW, Lee HJ, Choi GE, Jung YH, Kim JS, Lim JR, et al. High glucose-mediated PICALM and mTORC1 modulate processing of amyloid precursor protein via endosomal abnormalities. Br J Pharmacol 2020;177(16):3828—47. https://doi.org/10.1111/bph.15131.

[42] Vacínová G, Vejražková D, Lukášová P, Lischková O, Dvořáková K, Rusina R, et al. Associations of polymorphisms in the candidate genes for Alzheimer's disease BIN1, CLU, CR1 and PICALM with gestational diabetes and impaired glucose tolerance. Mol Biol Rep 2017;44(2):227—31. https://doi.org/10.1007/s11033-017-4100-9.

[43] Williamson A, Norris DM, Yin X, Broadaway KA, Moxley AH, Vadlamudi S, et al. Genome-wide association study and functional characterization identifies candidate genes for insulin-stimulated glucose uptake. Nat Genet 2023;vol. 55.

[44] Hoehn KL, Hohnen-Behrens C, Cederberg A, Wu LE, Turner N, Yuasa T, et al. IRS1-independent defects define major nodes of insulin resistance. Cell Metabol 2008;7(5):421—33. https://doi.org/10.1016/j.cmet.2008.04.005.

[45] Blot V, McGraw TE. GLUT4 is internalized by a cholesterol-dependent nystatin-sensitive mechanism inhibited by insulin. EMBO J 2006;25(24):5648—58. https://doi.org/10.1038/sj.emboj.7601462.

[46] Miller SE, Sahlender DA, Graham SC, Höning S, Robinson MS, Peden AA, et al. The molecular basis for the endocytosis of small R-SNAREs by the clathrin adaptor CALM. Cell 2011;147(5):1118—31. https://doi.org/10.1016/j.cell.2011.10.038.

[47] Williams D, Pessin JE. Mapping of R-SNARE function at distinct intracellular GLUT4 trafficking steps in adipocytes. J Cell Biol 2008;180(2):375—87. https://doi.org/10.1083/jcb.200709108.